Journal of
Marine Science and Engineering

MDPI

Article

Steady-State Motion of a Load on an Ice Cover with Linearly Variable Thickness in a Channel

Konstantin Shishmarev [1,†], Tatyana Khabakhpasheva [2,*,†] and Kristina Oglezneva [1,†]

[1] Department of Differential Equations, Altai State University, 656049 Barnaul, Russia
[2] Lavrentyev Institute of Hydrodynamics SB RAS, 630090 Novosibirsk, Russia
* Correspondence: tana@hydro.nsc.ru
† These authors contributed equally to this work.

Abstract: The paper considers the visco-elastic response of the ice cover in a channel under an external load moving with constant speed along the center line. The channel has a rectangular cross-section with a finite depth and width. The fluid in the channel is inviscid and incompressible and its motion is potential. The fluid is covered by a thin sheet of ice frozen to the channel walls. The ice thickness varies linearly symmetrically across the channel, being lowest at the center of the channel and highest at the channel walls. Ice deflections and strains in the ice cover are independent of time in the coordinate system moving with the load. The problem is solved numerically using Fourier transform along the channel and the method of normal modes across the channel. The series coefficients for normal modes are determined by truncation for the resulting infinite systems of linear algebraic equations. The ice deflections and strains in the ice plate are investigated and compared to the case of constant mean ice thickness. It is shown that even a small variation of the ice thickness significantly changes the characteristics of the hydroelastic waves in the channel.

Keywords: hydroelastic waves; moving load; frozen channel; linear thickness; ice deflections; strains

Citation: Shishmarev, K.; Khabakhpasheva, T.; Oglezneva, K. Steady-State Motion of a Load on an Ice Cover with Linearly Variable Thickness in a Channel. *J. Mar. Sci. Eng.* **2023**, *11*, 1045. https://doi.org/10.3390/jmse11051045

Academic Editors: Sarat Chandra Mohapatra and Carlos Guedes Soares

Received: 21 March 2023
Revised: 25 April 2023
Accepted: 6 May 2023
Published: 13 May 2023

1. Introduction

The problem of waves on ice cover was considered for the first time by Greenhill [1] and has been actively investigated since the sixties of the last century. The pioneering works on hydroelastic waves and the response of ice to moving loads were published in [2–4]. The main features of these waves were studied also later by Squire, V.A.; Hosking, R. and their group [5,6]. Very good reviews of these studies were made by Squire [5,7]. Only unbounded ice covers were considered that time. The ice sheet was modeled by an isotropic thin elastic plate. The water was assumed to be inviscid and incompressible. The dynamic equations describing this ice–water system were solved within the linear theory of hydroelasticity. This theory is relevant to this day. Models of thin elastic plates predict well the behavior of ice sheets with small thicknesses in the case of hydroelastic waves of small amplitude.

During the last 25 years, interest in ice cover has increased considerably, due to global warming as well as the possibility of wider use of the Arctic territories and natural reserves as well as use of the Northern Sea Route around of the year (see, for example [8]) on the one hand and the development of the Antarctic on the other.

Recent studies are focused on more specific problems of interaction between ice cover and coastal structures, such as walls (breakwaters), columns (supports of bridges and oil platforms), complex bottom topography, and channel walls. The problems of load moving near the ice sheet edge along the edge, between two ice sheets, on the liquid surface along the ice sheet edge, and many others have been considered, see in example [9,10]. Non-linear models of fluid–ice interactions have been studied numerically and analytically in [11,12]. Models that take into account the compressibility of ice were studied in [13–15]. These

models are used not only to describe the ice cover but also other floating elastic structures such as floating breakwaters and wave energy converters [16,17].

The behavior of an ice sheet with cracks has been studied during the last years. The solution for the scattering of an obliquely incident flexural–gravity wave by a narrow rectilinear crack separating two semi-infinite thin elastic plates floating on water of finite depth was obtained in [18]. The existence of localized edge waves traveling along the crack was discussed. The same authors generalized their solution to the case of a large number of cracks [19]. The problem of flexural–gravity waves in an ice sheet with a rectilinear crack generalized by a uniformly moving load was studied in [20]. The analytical solution was constructed. It was shown that in the case of both the plates having the same thickness and for the plate with the free edge near the vertical wall, at given special speed, there exist two edge wave modes with different wavenumbers. One of these waves propagates behind the load, and another one ahead of the load. The problem of a load moving along the frozen channel with a crack was studied in [21,22]. The main focus of the study was on the effect of a crack in the ice cover of a channel on strains and deflections of the ice sheet. The crack was placed at the center of the channel. It was shown that the ice deflections and strains along the crack are strongly dependent on the speed of the load and its relation to critical speed, i.e., minimum phase speed of the periodic hydroelastic waves propagating along the channel.

Models with damping (such as Kelvin–Voight models of ice) in the problems of load moving on an ice sheet were used by Zhestkaya and Kozin [23,24], by Brocklehurst [25] (chapter 5), and by Shishmarev et al. [26]. The dissipation effects, which are characterized by the retardation time in the Kelvin–Voigt viscoelastic model of an ice plate, were very strong in the numerical analysis by Zhestkaya and Kozin [24]. Investigation of the influence of retardation time on flexural–gravity waves in an ice channel with moving loads was done in [26]. There, you can find a good review of advantages and disadvantages of the Kelvin–Voigt model.

The present paper is about how ice with linearly changing thickness behaves under a moving load in a channel. The cross-section of the channel is rectangular because the majority of scientific and technical experiments with ice cover are conducted in ice tanks with such cross-sections. For this reason, studying the features of waves in channels and how they differ from waves in unbounded sheets is highly important. The boundary conditions at the channel walls significantly change the mathematical statement of the problem and affect the results of these studies. Investigations of waves in channels and their differences from the waves of the infinite extend as well as the hydroelastic behavior of the ice under the moving load were performed in the papers [26–29]. In contrast to the two-dimensional waves in the ice cover of infinite extend, there exists not only a system of propagating waves but also a number of sloshing waves across the channel. These waves have their own propagation speeds and critical speeds, which affect the waves system in the ice with moving loads.

In [30], the case of flexural–gravity waves propagation when ice thickness varies linearly across the channel was considered. The problem was solved by the normal mode method, where modes of plates with linear thickness were present analytically by functions found in [31]. Dispersion relations, profiles of flexural–gravity waves across the channel, and distributions of strain in the ice cover have been determined. It was shown that the behavior of flexural–gravity waves very much depends on the inclination parameter of the ice thickness and is different compared with those for a constant-thickness plate.

The present paper is concerned with the viscoelastic response of the ice cover in a channel caused by an external load moving with constant speed along the center line of the channel in the case when thickness of ice is linearly changed. The paper consists of several sections. In Section 2, the statement of the problem is formulated and the equations and variables are non-dimensionalized. The problem is solved within the linear theory of hydroelasticity. The formulation of the problem is similar to the one used in [28], but now the ice thickness linearly varies symmetrically across the channel, being the smallest at the

center of the channel and the largest at the channel walls. All considered cases of linear ice thickness satisfy the conditions of linear theory. The problem is formulated in such a way that the solution is sought in the coordinate system moving together with the load and does not depend on time. In Section 3, the solution method is described. The solution is based on the method of normal modes, into which the profile of ice oscillations across the channel is decomposed. The final solution for the ice deflections is obtained in the form of integrals using the inverse Fourier transform. Numerical results are described in Section 4. The ice deflections and strains in ice plates are investigated and compared with the case of a constant mean thickness of ice.

2. Formulation of the Problem

The response of a viscoelastic ice cover to a load moving along a frozen channel is considered. The channel is of rectangular section with a finite depth H ($-H < z < 0$) and a finite width $2b$ ($-b < y < b$), and the channel is of infinite extent in the x direction. Here, $Oxyz$ is a Cartesian coordinate system. The problem is studied within the linear theory of hydroelasticity (see, e.g., [5]). Liquid in the channel is inviscid, incompressible, and covered with ice. The ice cover is modeled by a thin viscoelastic plate with given constant density ρ_i and rigidity $D(y)$, where $D(y) = Eh_i^3(y)/[12(1-\nu^2)]$, E is the Young's modulus for ice, ν is the Poisson's ratio for ice, and $h_i(y)$ is the thickness of the ice cover. The ice thickness $h_i(y)$ is linear across the channel and symmetric with respect to a center line of the channel. The ice thickness is constant along the x direction.

The Kelvin–Voigt model of viscoelastic ice is used in this study. The constitutive equation of this model is $\sigma = E(\epsilon + \tau\partial\epsilon/\partial t)$, where σ is the stress, ϵ is the strain, τ is the so-called retardation time, and t is the time. Ice oscillations are caused by a load moving along the center line of the channel with constant speed U. The load is modeled by a localized smooth pressure distribution. Flow beneath the plate caused by ice deflections is potential. The scheme of the problem is shown in Figure 1.

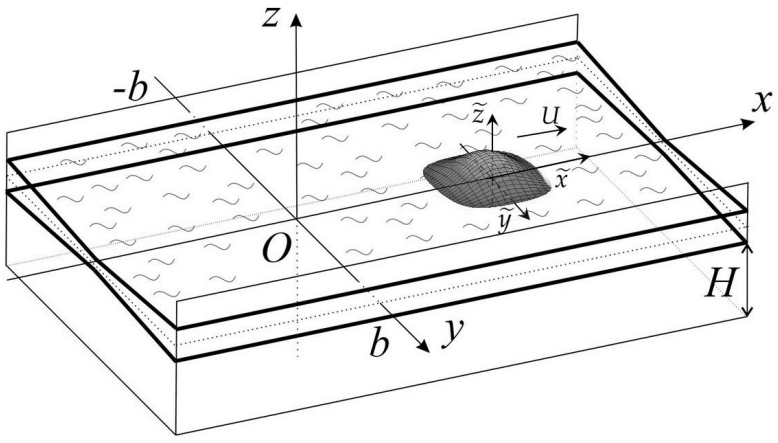

Figure 1. Scheme of the problem.

The ice deflection $w(x, y, t)$ satisfies the equation of a thin viscoelastic plate

$$M(y)\frac{\partial^2 w}{\partial t^2} + \left(1 + \tau\frac{\partial}{\partial t}\right)\Lambda w = p(x, y, 0, t) + P(x, y, t) \quad (-\infty < x < \infty, -b < y < b, z = 0), \tag{1}$$

where Λ is a differential operator,

$$\Lambda = D(y)\Delta^2 + 2D_y\left(\frac{\partial^3}{\partial y^3} + \frac{\partial^3}{\partial x^2 \partial y}\right) + D_{yy}\left(\frac{\partial^2}{\partial y^2} + \mu\frac{\partial^2}{\partial x^2}\right),$$

$\Delta^2 = \partial^4/\partial x^4 + 2\partial^4/\partial x^2\partial y^2 + \partial^4/\partial y^4$, $M(y) = \rho_i h_i(y)$ is the mass of the ice plate per unit area, $P(x, y, t)$ is the external pressure caused by the moving load, and $p(x, y, 0, t)$ is a

liquid pressure at the ice/liquid interface. If the ice thickness is constant, then $\Lambda = D\Delta^2$. The external pressure $P(x, y, t)$ moves along the center line of the channel with constant magnitude P_0 and is described by

$$P(x, y, t) = -P_0 P_1((x - Ut)/b) P_2(y/b) \quad (-\infty < x < \infty, -b < y < b), \tag{2}$$

$$P_1(\widetilde{x}) = \big(\cos(\pi c_1 \widetilde{x}) + 1\big)/2 \ \ (c_1|\widetilde{x}| < 1), \quad P_1(\widetilde{x}) = 0 \ \ (c_1|\widetilde{x}| \geq 1), \quad \widetilde{x} = (x - Ut)/b,$$

$$P_2(\widetilde{y}) = \big(\cos(\pi c_2 \widetilde{y}) + 1\big)/2 \ \ (c_2|\widetilde{y}| < 1), \quad P_2(\widetilde{y}) = 0 \ \ (c_2|\widetilde{y}| \geq 1), \qquad \widetilde{y} = y/b,$$

where c_1 and c_2 are non-dimensional parameters of the external load characterizing the size of the pressure area. The hydrodynamic pressure $p(x, y, 0, t)$ at the ice–liquid interface is given by the linearized Bernoulli equation,

$$p(x, y, 0, t) = -\rho_\ell \varphi_t - \rho_\ell g w \quad (-\infty < x < \infty, -b < y < b), \tag{3}$$

where g is the gravitational acceleration, ρ_ℓ is the density of the liquid, and $\varphi(x, y, z, t)$ is the velocity potential of the flow beneath the ice cover. The velocity potential $\varphi(x, y, z, t)$ satisfies Laplace's equation in the flow region and the boundary conditions

$$\varphi_y = 0 \ \ (y = \pm b), \quad \varphi_z = 0 \ \ (z = -H), \quad \varphi_z = w_t \ \ (z = 0). \tag{4}$$

We consider a case where the ice cover is frozen to the walls, which is modeled by the clamped conditions

$$w = 0, \quad w_y = 0 \qquad (-\infty < x < \infty, \ y = \pm b). \tag{5}$$

Other boundary conditions for the ice cover at the walls could be studied in the same way. The term with $\tau\partial/\partial t$ in the equation of the viscoelastic plate (1) describes the damping of ice plate oscillations so they decay far away from the moving load

$$w, \varphi \to 0 \quad |(x - Ut)| \to \infty. \tag{6}$$

Linear change in the ice thickness is considered: the ice thickness varies symmetrically across the channel, being the smallest at the center of the channel and the largest at the channel walls, see Figure 2. The main parameters of the thickness are its average h_* value and non-dimensional slope ratio α describing linear change of the ice thickness. Then, $h_i(y)$ can be written in the form

$$h_i(y) = h_0(1 + \alpha|y/b|), \tag{7}$$

where h_0 is minimum and h_1 is maximum values of the ice thickness

$$h_i(0) = h_0, \quad h_i(\pm b) = h_1, \quad h_1 = 2h_* \frac{1 + \alpha}{2 + \alpha} \quad h_0 = \frac{h_1}{1 + \alpha}.$$

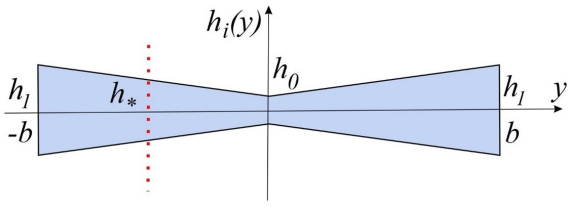

Figure 2. Shape of the ice cover across the channel.

The formulated problem is solved in non-dimensional variables denoted by tilde. The half-width of the channel b is taken as the length scale, the ratio b/U as the time scale, and the pressure magnitude P_0 as the pressure scale. The non-dimensional depth of the channel

H/b is denoted by h. The moving coordinate system $(\widetilde{x}, \widetilde{y}, \widetilde{z})$ with the origin at the center of the load is introduced by

$$\widetilde{y} = y/b, \quad \widetilde{x} = (x - Ut)/b, \quad \widetilde{z} = z/b, \quad \widetilde{t} = Ut/b.$$

We are concerned with a steady-state solution in the moving coordinate system,

$$w(x, y, t) = w(\widetilde{x}L + Ut, L\widetilde{y}, t) = w_{sc}\ \widetilde{w}(\widetilde{x}, \widetilde{y}),$$

$$\varphi(x, y, t) = \varphi(\widetilde{x}L + Ut, L\widetilde{y}, t) = \varphi_{sc}\ \widetilde{\varphi}(\widetilde{x}, \widetilde{y}, \widetilde{z}),$$

where w_{sc} and φ_{sc} are the scales of the ice deflection and the velocity potential, correspondingly. The scales are chosen as $w_{sc} = P_0/(\rho_\ell g)$ and $\varphi_{sc} = (UP_0)/(\rho_\ell g)$.

In the non-dimensional variables, the problem reads (tildes are omitted further)

$$m_0 h \mathrm{Fr}^2 h_i w_{xx} + \beta\left(1 - \varepsilon\frac{\partial}{\partial x}\right)\left[h_i^3\nabla^4 w + 6h_i^2 h_{i,y}(w_{yyy} + w_{xxy}) + 6h_i h_{i,y}^2(w_{yy} + \nu w_{xx})\right] + w$$
$$= h\mathrm{Fr}^2\varphi_x - P_1(x)P_2(y) \qquad (-\infty < x < \infty, \quad -1 < y < 1, \quad z = 0), \tag{8}$$

$$\nabla^2\varphi = 0 \qquad (-\infty < x < \infty, \ -1 < y < 1, \ -h < z < 0), \tag{9}$$

$$\varphi_z = -w_x \quad (z = 0), \qquad \varphi_y = 0 \quad (y = \pm 1), \qquad \varphi_z = 0 \quad (z = -h), \tag{10}$$

$$w = 0, \quad w_y = 0 \qquad (y = \pm 1), \qquad w, \varphi \to 0 \qquad (|x| \to \infty). \tag{11}$$

Here, $\beta = D_0/(\rho_l g b^4)$, $D_0 = Eh_0^3/[12(1 - \nu^2)]$, $\varepsilon = (\tau U)/b$, $m_0 = (\rho_i h_0)/(\rho_\ell b)$, and $\mathrm{Fr} = U/\sqrt{gH}$ is the Froude number.

The method for studying strains in the ice cover involves calculating the maximum strains in a plate. In the linear theory of hydroelasticity, strains change linearly with the thickness of the ice plate, and they are zero at the center of the plate [32]. Therefore, with respect to the plate thickness, the maximum strains occur at either the upper or lower surface. Only positive deformations, corresponding to elongation and stretching of the ice cover, are considered in this work. The strain tensor for the plate is

$$E(x, y) = -\zeta\begin{pmatrix} w_{xx} & w_{xy} \\ w_{xy} & w_{yy} \end{pmatrix}, \tag{12}$$

where ζ is a dimensionless coordinate along the thickness of the ice, with $-1 - \alpha y < \zeta < 1 + \alpha y$. Tensor (12) describes the strain field in the ice cover. To find the maximum strains, one needs to determine the eigenvalues of tensor (12) and select the maximum. In the linear theory of hydroelasticity, this method of analysis is correct if the condition $w_x^2 + w_y^2 \ll 1$ is satisfied and the strains do not exceed the critical value ϵ_{cr}. The critical value, or yield strain, of the material is defined as the value of deformation $\epsilon = \epsilon_{cr}$ at which the material starts to deform plastically. In this study, the value $\epsilon_{cr} = 8 \times 10^{-5}$ is used. This value of the yield strain has been used before, in particular in [25,26].

According to the introduced dimensionless variables, strains are scaled by the value of $h_0 w_{sc}/b^2$. Therefore, for different values of α, the value of h_0 and the scale of the strains will be different. Hence, all calculated dimensionless strains will be scaled by the value of h_r, where $h_r = h_0/h_*$. Thus, in any case, the dimensionless strains in the ice cover will be of the same scale equal to $h_* w_{sc}/b^2$, and the results for different cases of linear ice thickness can be compared in one figure.

The solution of the problem (8)–(11) depends on seven non-dimensional parameters, h, m, β, ε, Fr, c_1, and c_2, and on the parameters of the ice thickness h_* and α. These parameters describe the aspect ratio of the channel and characteristics of the ice and of the applied load. We shall determine the deflection w and strain distribution in the ice cover for given values of these parameters. A major aspect of the problem is the linear ice thickness. We shall

study the effect caused by the linearity of the thickness on the ice deflections and strains distribution. We keep average thickness h_* in all our calculations equal to one given value. Note that the scale of the ice thickness is equal to h_0 and will change in the calculations for different values of α. However, the scales of ice deflections and strains distribution do not depend on the scale of ice thickness, so they can be comparable while we do not change other scales.

3. Method of the Solution

The coupled problem (8)–(11) is solved with the help of the Fourier transform in the x direction. After applying the Fourier transform to (8)–(11), the plate Equation (8) provides

$$\beta(1-i\xi\varepsilon)\Big[h_i\Big[h_i^2 w^F_{yyyy}+6h_ih_{i,y}w^F_{yyy}+6h^2_{i,y}w^F_{yy}\Big] +h_i^3(\xi^4 w^F-2\xi^2 w^F_{yy})-6h_i^2h_{i,y}\xi^2 w^F_y-6h_ih^2_{i,y}\nu\xi^2 w^F\Big] + (1-m_0h\mathrm{Fr}^2\xi^2h_i)w^F = i\xi h\mathrm{Fr}^2\varphi^F-P^F(\xi,y), \quad (13)$$

where

$$w^F(\xi,y)=\frac{1}{\sqrt{2\pi}}\int_{-\infty}^{\infty}w(x,y)e^{-i\xi x}dx, \qquad w(x,y)=\frac{1}{\sqrt{2\pi}}\int_{-\infty}^{\infty}w^F(\xi,y)e^{i\xi x}dx. \quad (14)$$

Here, ξ is the parameter of the Fourier transform.

It is convenient to seek the Fourier image of ice deflections, $w^F(\xi,y)$, in the form of an infinite series of special spectral functions $\psi_n(y)$

$$w^F(\xi,y)=\sum_{n=1}^{\infty}a_n(\xi)\psi_n(y). \quad (15)$$

The spectral functions $\psi_n(y)$ are called normal modes of oscillations of a beam with linear thickness. They were calculated in [30] for consideration in this article for the case of the shape of ice thickness. The functions $\psi_n(y)$ are solutions of the spectral problem

$$h_i^2\psi_n+6h_ih_{i,y}\psi_n+6h^2_{i,y}\psi_n=\lambda_n^4\psi_n \quad (-1<y<1), \quad \psi_n(\pm1)=\psi_{n,y}(\pm1)=0. \quad (16)$$

The analytical solution of the differential equation in (16) can be obtained for polynomially varying thickness along the beam $(l+\gamma y)^k$. It was shown that for this varying thickness and rigidity of a beam behaving as $(l+\gamma y)^{3k}$, equations of oscillating plates can be reduced to Bessel's equations or Euler's equation [31]. For $k=1$, the general solution is

$$\psi_n(y)=\frac{1}{\zeta}[A_n\,J_1(\eta_n\zeta)+B_n\,Y_1(\eta_n\zeta)+C_n\,I_1(\eta_n\zeta)+D_n\,K_1(\eta_n\zeta)], \quad n=1,2,3\ldots \quad (17)$$

where $\eta_n=2\theta_n/\alpha$, $\zeta=\sqrt{h_i(y)}$, and J, Y, I, and K are Bessel functions. Parameters A_n, B_n, C_n, and D_n are determined from the boundary conditions and the normalization condition for the functions ψ_n.

It could be shown that both even and odd functions ψ_n are solutions of the differential equation in (16). Since we consider the load symmetric in y, we need to find only even modes. These modes satisfy conditions of zero slope and zero transverse shears of a beam

with linear thickness at its center. Therefore, these conditions and (16) give a system of equations for A_n, B_n, C_n, D_n, and η_n

$$A_n\,J_1(\eta_n\zeta_1) + B_n\,Y_1(\eta_n\zeta_1) + C_n\,I_1(\eta_n\zeta_1) + D_n\,K_1(\eta_n\zeta_+) = 0, \tag{18}$$
$$A_n\,J_0(\eta_n\zeta_1) + B_n\,Y_0(\eta_n\zeta_1) + C_n\,I_0(\eta_n\zeta_1) - D_n\,K_0(\eta_n\zeta_1) = 0, \tag{19}$$
$$A_n\,J_1(\eta_n\zeta_0) + B_n\,Y_1(\eta_n\zeta_0) + C_n\,I_1(\eta_n\zeta_0) + D_n\,K_1(\eta_n\zeta_0) - \eta_n\psi_{0n}(\zeta_0)/2 = 0, \tag{20}$$
$$\psi_{1n}(\zeta_0) - \eta_n\psi_{2n}(\zeta_0)/2 = 0, \tag{21}$$

where $\zeta_1 = \sqrt{h_i(1)}$, $\zeta_0 = \sqrt{h_i(0)}$, and

$$\psi_{0n}(\zeta_0) = A_n\,J_0(\eta_n\zeta_0) + B_n\,Y_0(\eta_n\zeta_0) + C_n\,I_0(\eta_n\zeta_0) - D_n\,K_0(\eta_n\zeta_0),$$
$$\psi_{1n}(\zeta_0) = -A_n\,J_1(\eta_n\zeta_0) - B_n\,Y_1(\eta_n\zeta_0) + C_n\,I_1(\eta_n\zeta_0) + D_n\,K_1(\eta_n\zeta_0),$$
$$\psi_{2n}(\zeta_0) = -A_n\,J_0(\eta_n\zeta_0) - B_n\,Y_0(\eta_n\zeta_0) + C_n\,I_0(\eta_n\zeta_0) - D_n\,K_0(\eta_n\zeta_0).$$

This system of Equations (18)–(21) is used to derive three of the four constants through the last one and find the spectral parameter η_n. This parameter is calculated as a value at which the corresponding matrix changes its sign. The functions $\psi_n(y)$ are orthogonal with respect to a weighted inner product, where the weight function is equal to $h_i(y)$

$$\int_{-1}^{1}(1+\alpha y)\psi_n(y)\psi_m(y)dy = 0 \qquad (n \neq m) \tag{22}$$

and A_n, B_n, C_n, and D_n are normalized in such a way that the integral in (22) is equal to 1 for $n = m$.

Using the transformed kinematic condition, $\varphi^F_z(\xi, y, 0) = -i\xi w^F(\xi, y)$, we seek the Fourier image of the flow velocity potential in the form $\varphi^F(\xi, y, z) = -i\xi\Phi(\xi, y, z)$,

$$\Phi(\xi, y, z) = \sum_{n=1}^{\infty} a_n(\xi)\phi_n(\xi, z, y), \tag{23}$$

where $\phi_n(\xi, z, y)$ is the solution of the following boundary problem

$$\frac{\partial^2\phi_n}{\partial y^2} + \frac{\partial^2\phi_n}{\partial z^2} = \xi^2\phi_n, \quad \frac{\partial\phi_n}{\partial z}(\xi, y, 0) = \psi_n(y), \quad \frac{\partial\phi_n}{\partial z}(\xi, y, -h) = 0.$$

By substituting (15) and (23) into (13), multiplying both sides of the result by $\psi_m(y)$, and integrating over y, we arrive at an infinite system of equations for principal coordinates $a_n(\xi)$

$$\beta(1 - i\xi\varepsilon)\left[a_m(\lambda_m^4 - 6h_{i,y}^2\xi^2\nu) + 2\xi^2\sum_{n=1}^{\infty}a_nS_{nm} + \xi^4\sum_{n=1}^{\infty}a_nK_{nm}\right]$$
$$-a_m m_0 h\mathrm{Fr}^2\xi^2 + \sum_{n=1}^{\infty}a_nM^{(1)}_{nm} - h\xi^2\mathrm{Fr}^2\sum_{n=1}^{\infty}a_nM^{(2)}_{nm} = P_m, m = 1, 2, 3, \ldots \tag{24}$$

where

$$S_{nm} = \int_{-1}^{1} h_i^3\psi_n'\psi_m'dy, \quad K_{nm} = \int_{-1}^{1} h_i^3\psi_n\psi_m dy, \quad M^{(1)}_{nm} = \int_{-1}^{1}\psi_n\psi_m dy,$$

$$M^{(2)}_{nm} = \int_{-1}^{1}\phi_n(\xi, y, 0)\psi_m dy, \quad P_m = -\int_{-1}^{1}P^F\psi_m dy.$$

Algebraic problem (24) can be written in the matrix form

$$\left(\beta(1-i\xi\varepsilon)\left[\mathbf{D}+2\xi^2\mathbf{S}+\xi^4\mathbf{K}\right]-m_0h\mathrm{Fr}^2\xi^2\mathbf{I}+\mathbf{M}^{(1)}-h\xi^2\mathrm{Fr}^2\mathbf{M}^{(2)}\right)\vec{a}=\vec{P}, \tag{25}$$

where $\mathbf{D}$ is a diagonal matrix with elements $(\lambda_m^4-6h_{i,y}^2\xi^2\nu)$, $\mathbf{S}=\{S_{nm}\}$, $\mathbf{K}=\{K_{nm}\}$, $\mathbf{M}^{(1)}=\{M_{nm}^{(1)}\}$, $\mathbf{M}^{(2)}=\{M_{nm}^{(2)}\}$, $\mathbf{I}$ is an identity matrix, and $\vec{P}$ is a vector with elements P_m. It can be shown that all matrices in (25) are symmetric. To solve matrix equation (25), we reduce the number of modes $\psi_n(y)$ to a finite number N_{mod} and distinguish the real and imaginary parts of the vector $\vec{a}$, $\vec{a}=\vec{a}^R+i\vec{a}^I$. All vectors and elements of the matrices in the obtained equation are real, which provides the system with two non-homogeneous matrix equations with respect to $\vec{a}^R$ and $\vec{a}^I$. In the present problem, $P_1^F(\xi)$ is an even function of ξ. It can be shown that $a_n^R(\xi)$ are even and $a_n^I(\xi)$ are odd functions of ξ.

The ice deflection $w(x,y)$ is obtained by the inverse Fourier transform, see the second equation in (14),

$$w(x,y)=\frac{\sqrt{2}}{\sqrt{\pi}}\sum_{n=1}^{Nmod}\psi_n(y)\int_0^\infty a_n^R(\xi)\cos(\xi x)-a_n^I(\xi)\sin(\xi x)d\xi. \tag{26}$$

The area of integration in (26) is limited by N_ξ, and the number of integration steps is equal to N. Functions $a_n^R(\xi)$ and $a_n^I(\xi)$ are approximated by linear functions, and the resulting integrals are calculated analytically for each mode. The convergence of the numerical solution is checked by varying the number of modes and the integration parameters. For a plate of constant thickness, the solution method is similar to the method used in [26].

4. Numerical Results

Calculations of the ice response were carried out for parameters of the problem corresponding to the experimental ice tank at the Sholem Aleichem Amur State University in Birobidzhan (see [33]): $H=1$ m, $2b=3$ m, ice thickness in the tank is chosen to be equal to 0.0035 m. The parameters of ice and liquid in the calculations were $\rho_i=917$ kg/m^3, $\rho_\ell=1024$ kg/m^3, $\mu=0.3$, $E=4.2\times10^9$ Pa, and $\tau=0.1$ s. The slope ratio of the linear change of ice thickness α and the speed of the load U change in the calculations. The average thickness h_* in all calculations did not change and is equal to 0.0035 m. All results presented further are shown in non-dimensionless variables unless otherwise specified, and tildes are omitted.

Precision of calculations depends on the parameter of integration, N_ξ, N, and number of modes N_{mod}. A series of test calculations show that $N_{mod}=10$ is enough to obtain the numerical results with visual accuracy. A sufficient range of the parameters of integration were tested on a series of calculations with successively increasing the number of steps and the interval of integration. When the slope ratio of the ice thickness α tends to 0, the ice plate with linear thickness becomes more flattened, being a plate with constant thickness at the limit. Small amounts of α lead to high values of η_n in (17), and $\eta_n\to\infty$ as $\alpha\to0$. Therefore, it is impossible to calculate the spectral parameters η_n, modified Bessel functions I_n, and, correspondingly, the ice deflections $w(x,y)$ for small α. It is expected that all results for a plate with linear thickness tend to results for a plate with constant thickness as $\alpha\to0$. The results for a plate with constant thickness can be calculated by the method described in [26]. Convergence of characteristics of periodic hydroelastic waves propagating along a frozen channel was investigated in [30].

Comparison of the results for the plate with slowly changing linear thickness and for the plate with constant thickness are shown in Figure 3. Non-dimensional ice deflections along the center line of the channel are shown in Figure 3a, and strains are shown in Figure 3b. The results for the plate with linear thickness are shown by a dashed red line, and for the plate with constant thickness by a black solid line. The results in the figures are calculated for $U = 1.5$ m/s and $\alpha = 0.05$. This slope ratio corresponds to $h_0 \approx 0.0034$ m and $h_1 \approx 0.0036$ m, which is a very small change in the ice thickness over the 1.5 m length of the plate. The ice deflections and strains for both cases are visually matched. There are few deviations near the center of the load, $x = 0$. In general, the ice plate with a very small change in linear thickness can be approximated by the plate with constant thickness.

However, when making such an approximation, one must be careful with the calculation error of the strains. The accuracy of the strain distribution calculation is more important than the accuracy of the ice deflections due to the estimation of possible ice breaking. The maximum difference in strains, $|\varepsilon^{(c)} - \varepsilon^{(l)}|$, calculated as a function of U, is shown in Figure 4a for strains along the central line of the channel and in Figure 4b for strains at the walls. Notation $^{(c)}$ means strains calculated for a plate with constant thickness and $^{(l)}$ is for a plate with linear thickness with $\alpha = 0.05$. Since we are discussing the accuracy of approximating an ice plate with nearly constant linear thickness by a plate with constant thickness, in this paragraph, we will refer to the difference in calculated strains as the calculation error. Overall, the error in dimensionless values is small. The first critical speed at which the load begins to generate hydroelastic waves in the ice cover is slightly less than 2 m/s. Once the hydroelastic waves start to contribute to the reaction of the ice cover to the load (values at $U \geq 2$ on the graphs), the error in the calculated strains at the walls increases. The error in strains along the central line of the channel where the load is located is generally at the level of 0.07 dimensionless values with small fluctuations.

The maximum absolute error in the calculated strains for the plate approximated by one with constant thickness depends on the parameters of the strain scale, ε_{sc}. For example, at a speed of $U = 2$ m/s, the maximum dimensionless strains in the ice cover with linear thickness are reached in the area near the load and are approximately equal to 2.45. The critical value of P_0 at which the ice will begin to break, i.e., the dimensional strains reach the value of ε_{cr}, is approximately 377 Pa. Therefore, the maximum error in dimensionless strains when approximating a plate with constant thickness is 0.085. For the given load amplitude, the value of this error will be no more than 3.5 percent of the critical value. Note that this is the maximum possible error; in other cases, the error will be smaller. Therefore, taking into account this error estimate, the strains distribution in the ice plate with nearly constant linear thickness can be approximated by the strains distribution for the plate with constant thickness.

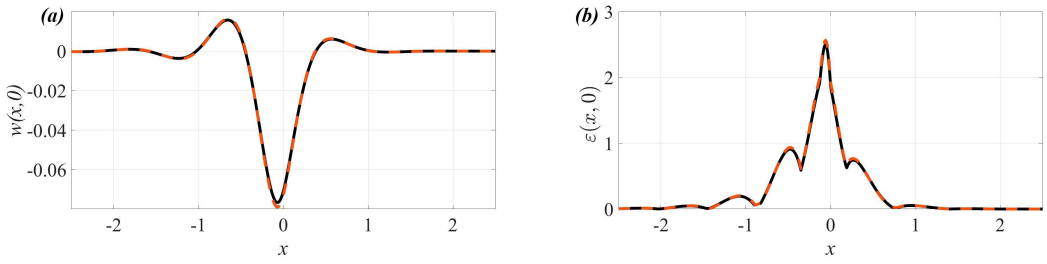

Figure 3. Non-dimensional ice deflections (**a**) and strains (**b**) along the center line of the channel for $U = 1.5$ m/s and $\alpha = 0.05$. The results for the plate with linear thickness are shown by a dashed red line and for the plate with constant thickness by a black solid line.

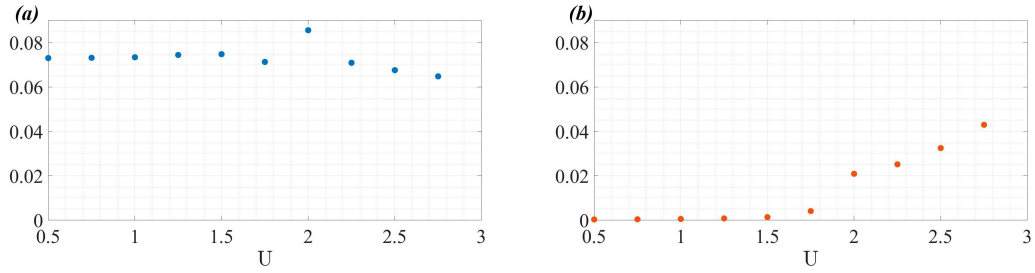

Figure 4. Maximum of $|\varepsilon^{(c)}(x,0) - \varepsilon^{(l)}(x,0)|$ as a function of U (**a**) and maximum of $|\varepsilon^{(c)}(x,1) - \varepsilon^{(l)}(x,1)|$ as a function of U (**b**), where notation $^{(c)}$ means strains calculated for a plate with constant thickness and $^{(l)}$ is for the plate with linear thickness with $\alpha = 0.05$.

The first series of calculations for the ice deflections and strains in the ice cover were performed for the thickness parameters of the ice cover specified in Table 1 and for $U = 1.5$ m/s. This speed is less than the minimum phase speed of periodic hydroelastic waves propagating along the ice cover with a constant thickness. In this case, the presence of hydroelastic waves that form deflections in the ice cover is not expected, and the ice deflections are usually formed only in a small area under the load. Dimensionless ice deflections are shown in Figure 5a. Here and further, on graphs plotted along the x-axis, the center of the external load is located at $x = 0$ and the load moves from left to right. Dimensionless and scaled by the maximum absolute value, the ice deflections across the channel are shown in Figure 5b. Dimensionless strains are shown in Figure 6a along the center line of the channel and in Figure 6b at the walls. Note that dimensionless strains for ice with a linear thickness are scaled by the value h_0/h_z so that the scale of the dimensionless results coincides. The results for an ice cover with a constant thickness are shown by black, and the results for an ice cover with a linearly changing thickness by colored lines (see Table 1). The "Red" case is a slight change in thickness, wherein the ice thickness increases linearly by two times. Qualitatively, the shapes of the ice deflections and strains have not changed. The amplitudes of the ice deflections and strains along the line of motion of the load have increased slightly, approximately by two times. At the walls, away from the load, the strains have not changed, despite the fact that the thickness of the ice at the walls has increased by 1.3 times. In the "Violet" case, the ice thickness increases by 11 times. In this case, the ice deflections have a wave profile. This is due to the fact that for a channel with such a thickness, dispersion relations and phase speeds of hydroelastic waves possibly propagating along the channel have changed. At the same time, the wave is observed only behind the load. Waves in front of it are damped due to the relatively high viscosity of the considered ice, $\tau = 0.1$ s. Increasing the α parameter (increasing the change in the ice thickness) narrows the area of oscillations across the channel, i.e., the ice oscillates with larger amplitudes where its thickness becomes smaller and oscillates less in sections with increased thickness, in the considered case, at the walls. At the same time, the curvature of the ice deflections (see Figure 5b) and, therefore, the strains in the ice cover increase at the bend. In the transverse profile of the ice deflections, the contribution of the first mode $\psi_1(y)$ is clearly observed. The corresponding values of the external load magnitude, P_0, required to break the ice are 337 Pa in the black case, 182 Pa in the "Red" case, and 33 Pa in the "Violet" case.

Table 1. Parameters of the ice thickness used in the calculations.

Case	Type	α	h_0	h_1	h_z
Black	Constant thickness	0	0.0035 m	0.0035 m	0.0035 m
Red	Linear thickness	1	0.0023 m	0.0047 m	0.0035 m
Violet	Linear thickness	10	0.00058 m	0.0064 m	0.0035 m

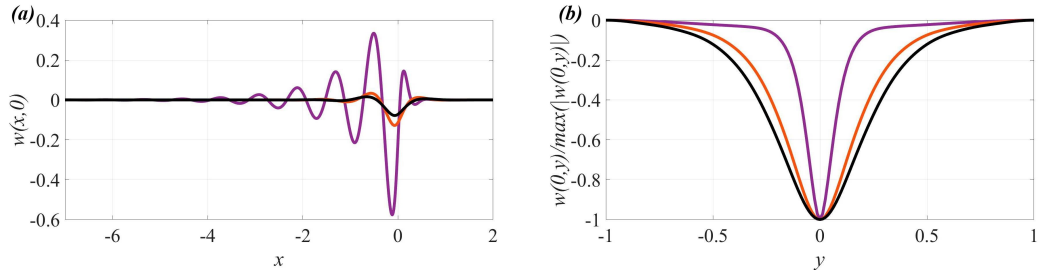

Figure 5. Non-dimensional ice deflections along the center line of the channel (**a**) and normalized ice deflections across the channel (**b**) for $U = 1.5$ m/s. The results for the plate with linear thickness are shown by colored lines, for the plate with constant thickness—by a black line (for the legend see Table 1).

The behavior of the ice cover strongly depends on the speed of the load and its relationship to the phase speeds of periodic hydroelastic waves propagating along the ice cover. The deflection of the ice cover typically consists of the local ice response to the moving load and a system of hydroelastic waves propagating from the load. The number of such waves is equal to the number of periodic waves whose phase speed equals to the speed of the moving load. Linear changes in ice thickness can greatly affect the characteristics of these periodic waves. Therefore, the number of waves contributing to the formation of ice deflection can vary. The first three phase speeds for symmetric waves propagating along the channel with the lowest frequencies are shown in Figure 7 for the black and "Violet" cases from Table 1. If a horizontal line denoting the speed of the load, in this case $U = 1.5$ m/s, is drawn, it can be seen that the intersection points of the phase speeds and load speed exist in the "Violet" case, but are absent in the black case. This explains the qualitative change in the shape of the ice deflections in Figure 5. Despite a large change in the ice thickness in non-dimensional variables, in dimensional variables, the angle of inclination of the ice surface is only $\approx 0.0019^\circ$. In reality, such a change in the ice thickness is difficult to notice visually, but the characteristics of the ice response to the moving load change significantly (see Figures 5 and 6a). Another important characteristic is the critical speed of the moving load, which is equal to the minimum of phase speed. When the load moves at this speed, within the framework of linear theory without damping, the deflections of the ice will be unbounded. In the framework of theory with viscosity, it is expected that the deflections and strains of the ice will have the largest amplitude when the load moves at the critical speed. The linear thickness of the ice cover also changes the values of critical speeds. The corresponding critical speeds as functions of the parameter α are shown in Figure 7b. It can be seen that with an increase in the linear change in the ice thickness, the critical speeds decrease due to the appearance of thin sections in the ice cover. The critical speeds change faster for small values of α. As α increases, the rate of change of critical speeds decreases.

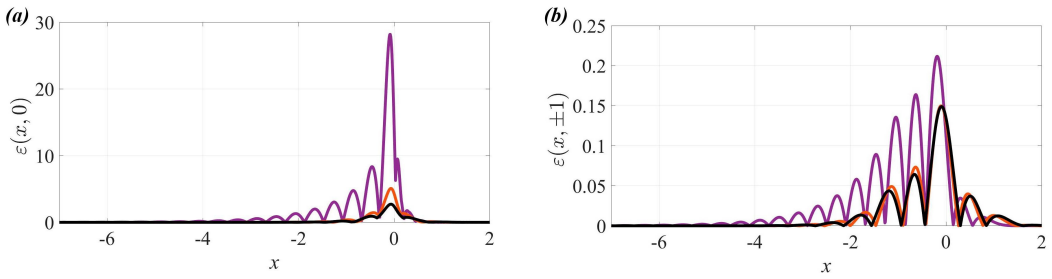

Figure 6. Non-dimensional strains along the center line of the channel (**a**) and at the walls (**b**) for $U = 1.5$ m/s. The results for the plate with linear thickness are shown by colored lines and for the plate with constant thickness by a black line (for the legend, see Table 1).

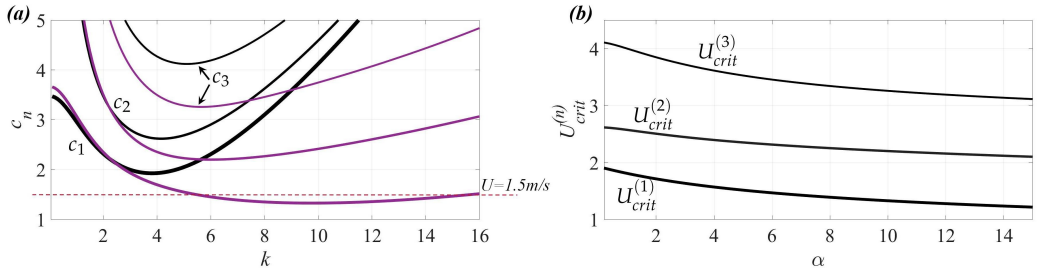

Figure 7. Phase speeds of the first three symmetric hydroelastic waves propagating along the channel with the lowest frequencies (**a**). The corresponding critical speeds as functions of the parameter α (**b**). Black and violet lines correspond to "Black" and "Violet" cases, see Table 1.

Results similar to those presented in Figures 5 and 6 but for the speed of the load $U = 2.5$ m/s are shown in Figures 8 and 9. These results also correspond to the cases described in Table 1. The speed $U = 2.5$ m/s is a supercritical speed for the considered channel. The supercritical speed means that it is greater than the first minimum phase speed of the periodic hydroelastic waves propagating in the considered channel. However, for the considered ice with constant thickness, this speed is less than the second minimum phase speed. In the "Violet" case, where the linear change in thickness is largest, the speed $U = 2.5$ m/s is higher than both the first and second minimum phase speeds (see Figure 7). Non-dimensional ice deflections along the central line of the channel are shown in Figure 8a. It is known that when a load moves in the channel, it can generate hydroelastic waves, and long waves propagate behind the load, while short waves propagate ahead [26]. In the considered case, only long waves behind the load are observed, see Figure 8a. The observed ice deflections correspond to a hydroelastic wave propagating with a phase speed c_1, i.e., the first hydroelastic wave with the lowest frequency. The phase speeds and wavelengths of these waves change very slightly for the considered cases of the linear ice thickness, see Figure 7 for c_1 when $k < 3$ m^{-1}. However, in the last figure, it can be seen that for the same speed, the wave number k is slightly higher in the "Violet" case. Therefore, the wavelength of the wave generated by the load in the "Violet" case should be slightly smaller than that of the wave in the ice cover with constant thickness. Accordingly, this change in wavelength is observed in Figure 8a for $x < -2$. It should be noted that it is visually impossible to observe the appearance of short waves ahead of the load. It is also hard to note the appearance of the second long hydroelastic wave behind the load in the "Violet" case, except for small oscillations of the ice deflections near the load at $x = -1$. It is assumed that the absence of short waves ahead and the second long wave behind the load in the distance (at $x < -2$) corresponding to the second hydroelastic wave are caused by the large damping of oscillations for the considered characteristics of the ice cover. Due to the reduction of ice thickness at the center of the channel, the maximum strains increase directly under the load. Note that the reduction of ice thickness in the considered linear symmetric case does not significantly affect the amplitudes of hydroelastic waves at a distance from the load.

Normalized ice deflections in the cross-section of the channel, scaled by their maximum value and plotted through the center of the moving load, $y = 0$, are shown in Figure 8b. A similar narrowing of the ice deflections closer to the center line, where the ice becomes thinner, is noted as in the previous case for $U = 1.5$ m/s. The obtained results show that the main contribution to the formation of the ice deflections across the channel is made by the normal mode $\psi_n(y)$, corresponding to the hydroelastic wave, whose minimal phase speed, among other minimum phase speeds, is closest to the speed of the load. In the case of $U = 1.5$ m/s, this normal mode is $\psi_1(y)$, and in the case of $U = 2.5$ m/s, this is $\psi_2(y)$. This conclusion holds for both the ice cover with constant thickness and the ice cover with linearly varying thickness.

The maximum dimensionless strains are shown along the center line of the channel and at the walls in Figure 9a,b. The strains along the center line of the channel increase with

increasing parameter α, which is in good agreement with the previous case for $U = 1.5$ m/s. Considering the values of strains in both cases of the speed of the load, the strains will be maximum for the "Violet" case for $U = 1.5$ m/s. Note that for the speed $U = 1.5$ m/s, in this case, hydroelastic waves appear and propagate in the ice cover due to large linear changes in the ice thickness. The relative reduction of these strains in the "Violet" case for $U = 2.5$ m/s, in which hydroelastic waves are also generated by the load, shows the importance of the first mode in the considered problems. The opposite situation is observed for the strains at the walls. The maximum strains here are observed for the ice cover with constant thickness. The strains at the walls for the speed $U = 2.5$ m/s are greater than those for $U = 1.5$ m/s. However, strains along the center line of the ice cover with linearly varying ice thickness are one order of magnitude greater than the strains at the walls for both cases of the speed of the load.

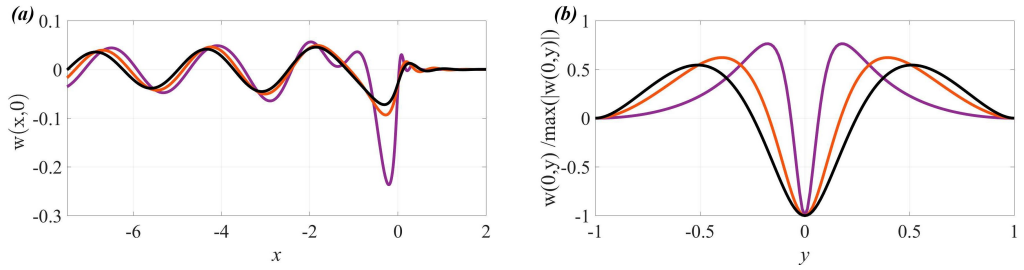

Figure 8. Non-dimensional ice deflections along the center line of the channel (**a**) and normalized ice deflections across the channel (**b**) for $U = 2.5$ m/s. The results for the plate with linear thickness are shown by colored lines and for the plate with constant thickness by a black line (for the legend, see Table 1).

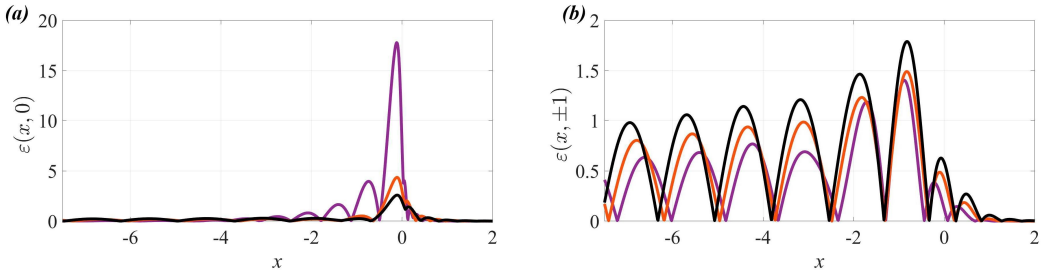

Figure 9. Non-dimensional strains along the center line of the channel (**a**) and at the walls (**b**) for $U = 2.5$ m/s. The results for the plate with linear thickness are shown by colored lines and for the plate with constant thickness by a black line (for the legend, see Table 1).

The maximum positive and minimum negative dimensionless ice deflections along the central line of the channel are shown in Figure 10a. Results for $U = 1.5$ m/s are shown by blue lines. Results for $U = 2.5$ m/s are shown by red lines. The results for the subcritical speed, $U = 1.5$ m/s, show a monotonic increase in the absolute values of deflections with an increase in the linear change in ice thickness. In the case of supercritical speed, the amplitudes of deflections increase much more slowly. The maximum absolute deflections are always observed under the load and, in the considered cases, are always negative. Note that for the speed $U = 1.5$ m/s, there is a value of α at which $U(\alpha) = \min(c_1)$, where $\alpha_* \approx 5.5$, see Figure 7b. Despite the appearance of hydroelastic waves in the case of $U = 1.5$ m/s at $\alpha > 5.5$, the amplitudes of deflections continue to increase faster than in the case of $U = 2.5$ m/s. The minimum magnitudes of the external load P_0 that lead to the destruction of the ice cover as a function of the parameter α are shown in Figure 10b. The magnitudes decrease with an increase in the parameter α. The behavior of magnitudes is the same for both considered cases, $U = 1.5$ m/s and $U = 2.5$ m/s. Magnitudes are smaller for the first, subcritical case. Note that the values of P_0 are inversely proportional to the dimensionless strains ε. With an increase in the parameter α, the magnitudes visually

begin to approach an asymptotic value. This is due to the fact that the parameter α is inversely proportional to the value of the ice thickness at the center of the channel h_0, $h_0 = 2h_*/(2+\alpha)$. Therefore, the larger the value of the parameter α, the lower the thickness of the ice in the center and, consequently, the bending rigidity of the ice decreases. This confirms the fact that strains and stresses in the ice cover change more significantly for the initial segment of α. The maximum dimensionless strains are shown as functions of the parameter α in Figure 11. The maximum strains along the central line of the channel monotonically increase in both cases. In the case of $U = 1.5$ m/s, the growth is faster. At the walls, the strains are changed very slowly with an increase in the parameter α. Overall, since the external load moves along the central line, where the ice becomes thinner, and away from the walls, where the ice becomes thicker, the strains at the walls have an insignificant role. For all considered values of the parameter α, the strains at the walls in the supercritical case of $U = 2.5$ m/s are greater than in the subcritical case of $U = 1.5$ m/s.

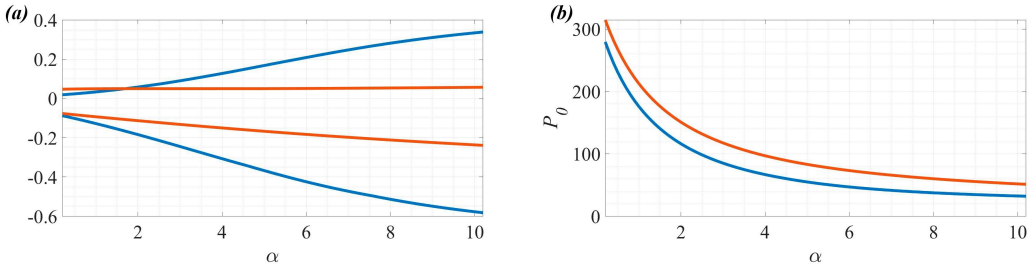

Figure 10. Maximum positive and minimum negative ice deflections along the center line of the channel as functions of α (**a**). Minimum magnitude P_0 possibly leading to ice breaking as function of α (**b**). Results for $U = 1.5$ m/s are shown by blue lines. Results for $U = 2.5$ m/s are shown by red lines.

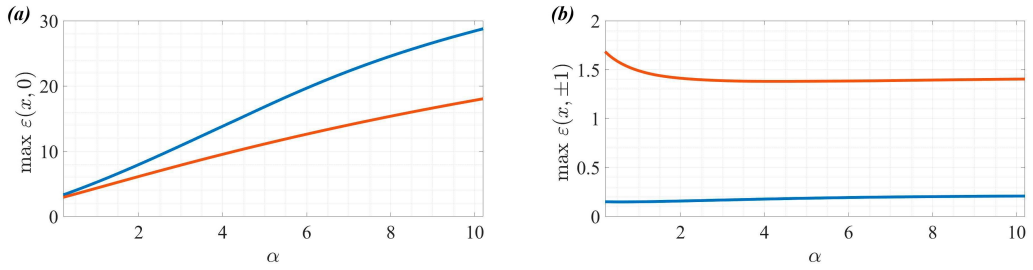

Figure 11. Maximum non-dimensional strains along the center line of the channel as functions of α (**a**). Maximum non-dimensional strains at the walls of the channel as functions of α (**b**). Results for $U = 1.5$ m/s are shown by blue lines. Results for $U = 2.5$ m/s are shown by red lines.

In the linear theory for the speed of the load $U = min(c_1)$, it is predicted that the ice deflections and strains in the ice cover will be unbounded. In the case of an ice cover with viscous effects, it is expected that the ice deflections and strains will be maximum for this speed of the load. These conclusions were obtained for an ice cover of constant thickness. As mentioned earlier, $\alpha \approx 5.5$ when $U = min(c_1)$. Therefore, maximum ice deflections and strains shown in Figures 10 and 11 were expected to be observed at $\alpha = \alpha_*$ if the critical velocity theory works for an ice cover of variable thickness. However, all the presented results are monotonic for $0 < \alpha < 10$. This may be due to the high viscosity of the considered characteristics of the ice cover. Results for $\tau = 0.1$ s and $\tau = 0.01$ s are shown in Figures 12 and 13 for $U = 1.5$ m/s. Results for $\tau = 0.1$ s are shown by solid lines. Results for $\tau = 0.01$ s are shown by dot-dashed lines. Indeed, maximum ice deflections, strains, and minimum amplitudes of external load required to break the ice are observed in the vicinity of $\alpha \approx 5.5$. Visually, ice deflections begin to differ at $\alpha > 2$, and strains and magnitudes differ for all α. Further increase in α, despite the fact that the ice at the line

of load motion becomes thinner, does not lead to such ice deflections and strains whose amplitudes are higher than in the critical case of $\alpha = \alpha_*$.

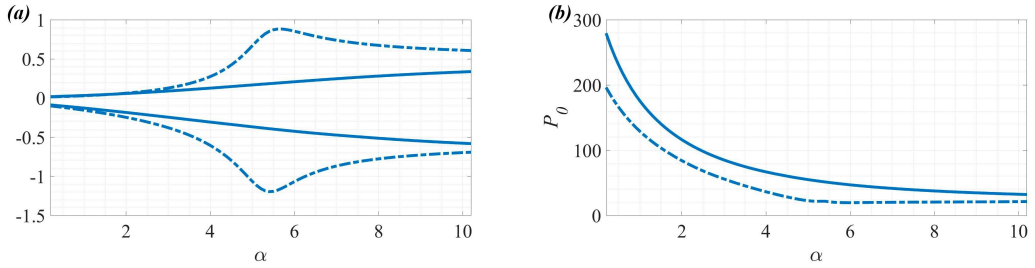

Figure 12. Maximum positive and minimum negative ice deflections along the center line of the channel as functions of α (**a**). Minimum magnitude P_0 possibly leading to ice breaking as function of α (**b**). Results for $\tau = 0.1$ s are shown by solid lines. Results for $\tau = 0.01$ s are shown by dot-dashed lines. Results presented here are for $U = 1.5$ m/s.

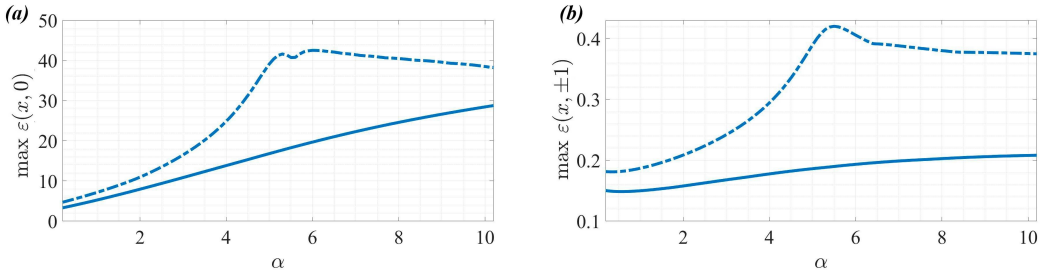

Figure 13. Maximum non-dimensional strains along the center line of the channel as functions of α (**a**). Maximum non-dimensional strains at the walls of the channel as functions of α (**b**). Results for $\tau = 0.1$ s are shown by solid lines. Results for $\tau = 0.01$ s are shown by dot-dashed lines. Results presented here are for $U = 1.5$ m/s.

5. Conclusions

The problem of an external load moving with constant speed along the central line of a frozen channel was investigated. The ice thickness was varying symmetrically across the channel by a linear law, being smallest at the center of the channel and highest at the channel walls. The external load was modeled by a smooth, localized pressure spot. The problem was solved within the linear theory of hydroelasticity. The problem parameters were chosen in such a way that the dimensions of the channel and ice characteristics correspond to the experimental ice tank described in [33]. The problem was solved by the coordinate system moving together with the load. The ice deflections and strains, which were assumed independent of time in this coordinate system, were investigated.

The main parameter whose influence on the ice response was investigated in the present study was the parameter α describing the slope of the profile of the ice thickness in dimensionless variables. Increasing this parameter gives a decrease in the ice thickness at the center of the channel and an increase in the thickness at the walls. When $\alpha = 0$, the ice thickness is constant. The normal modes for a linear thickness plate presented here, cannot be constructed at $\alpha = 0$. In this case, the modes that were used for the constant thickness plate in [26] must be applied. The results obtained in the present paper have been verified by comparing them at small alpha with the results received by modes from [26].

It is known that the response of the ice cover to a moving load is formed as a sum of local deflections under the load and a system of hydroelastic waves propagating from the load [28]. A change in the parameter α changes the characteristics of these hydroelastic waves. New hydroelastic waves propagating from the load may appear as the linear change in ice thickness increases. For the considered conditions, the hydroelastic waves in the channel become shorter when α increases. The ratio of the speed of the load to the critical speeds (minimum phase speeds of periodic hydroelastic waves) is of great importance.

Changing the ice thickness can change this ratio, as increasing the parameter α reduces the minimum phase speeds. Therefore, if the load was moving at a subcritical speed over an ice cover of constant thickness, the current speed of the load may become critical or even supercritical when it enters an area of varying ice thickness. Then, hydroelastic waves propagating from the load will appear in the ice cover, and the ice deflections and strains in the ice will change significantly.

The load speeds 1.5 m/s and 2.5 m/s have been used in calculations. For the ice cover with constant thickness $h_{ice} = 3.5$ mm, these speeds are subcritical and supercritical, respectively. The ice deflections and strains in the ice cover were investigated for $0 < \alpha \leq 10$ and mean thickness $h_z = 3.5$ mm. It has been shown that for both speeds, the maximum deformation is achieved along the center line of the channel, where the ice thickness is minimal. Deformation on the walls is higher in the subcritical case, despite the increase in ice thickness on the walls, and lower in the supercritical case. However, in both cases, the strains along the center line are still an order of magnitude greater than they are near the walls. The maximum strains among all considered cases were observed in the subcritical case for large α. In the supercritical case, increasing α reduces the length of hydroelastic waves propagating from the load but has almost no effect on the amplitude of the waves far from the load.

Investigation of the deflection profiles across the channel showed the expected shrinking of oscillations towards the center of the channel, where the ice becomes thinner. Despite the increased curvature of the deflections, maximum strains are always expected under the load, in the region of the smallest ice thickness. The minimum external load magnitudes required for the ice to break are inversely proportional to the parameter α. For $\alpha = 10$, the magnitudes can decrease by 10 times.

The effect of damping within the Kelvin–Voight model in combination with linearly varying ice thickness is investigated. It is expected that as the α parameter increases, the minimum phase speeds will decrease and, at some instant, reach the speed of the load. In this case, the linear theory predicts that the ice deflections and strains in the ice cover will be maximal. For the considered channel, the value of the retardation time parameter $\tau = 0.1$ s turned out to be very large. There is an increase of parameter α, up to the moment when the minimum of the first phase velocity $min(c_1)$ becomes equal to $U = 1.5$ m/s, which further leads only to monotonic increase of the ice deflections and strains in the ice cover. For $\tau = 0.01$ s, the maximum deflections and strains in the ice cover are observed at $\alpha \approx 5.5$, and further increase in α leads to a decrease in the deflections and strains.

The possibility of approximating a plate with linear varying thickness by a plate with constant thickness in problems with moving loads was investigated. For very small values of parameters of linearity, $\alpha = 0.05$, the deflections and strains are visually equal to those for the constant mean thickness case. The error in dimensional strains depends on the magnitude of the external load and can be no more than three percent. For larger values of the external load magnitude, the error will be larger but the linear theory is no longer applicable.

Author Contributions: Conceptualization, T.K. and K.S.; methodology, T.K. and K.S.; software, K.S.; validation, K.S. and K.O.; formal analysis, T.K., K.S., and K.O.; investigation, K.S. and K.O.; resources, T.K. and K.S.; writing—original draft preparation, K.S. and K.O.; writing—review and editing, K.S. and T.K.; and visualization, K.O. All authors have read and agreed to the published version of the manuscript.

Funding: The study was funded by RFBR and TUBITAK according to the research project—20-58-46009 Loads on engineering structures in sea ice.

Institutional Review Board Statement: Not applicable.

Informed Consent Statement: Not applicable.

Data Availability Statement: Data of numerical calculations are available upon request.

Conflicts of Interest: The authors declare no conflict of interest.

References

1. Greenhill, A.G. Wave motion in hydrodynamics. *Am. J. Math.* **1886**, *9*, 62–96. [CrossRef]
2. Kheysin, Y. Moving load on an elastic plate which floats on the surface of an ideal fluid. *Izv. Akad. Nauk SSSR Otd. Tekh. Nauk Mekh. i Mashinostr.* **1963**, *1*, 178–180. (In Russian)
3. Sabodash, P.F.; Filippov, I.G. A dynamic problem for a thin elastic plate. *Int. Appl. Mech.* **1967**, *3*, 28–31. [CrossRef]
4. Nevel, D.E. *Moving Loads on a Floating Ice Sheet*; US Army Cold Regions Research and Engineering Lab.: Hanover, NH, USA, 1970; No. CRREL-RR-261.
5. Squire, V.A.; Hosking, R.; Kerr, A.; Langhorne, P.J. *Moving Loads on Ice Plates*; Kluwer: Dordrecht, The Netherlands, 1996.
6. Hosking, R.J.; Sneyd, A.D.; Waugh, D.W. Viscoelastic response of a floating ice plate to a steadily moving load. *J. Fluid Mech.* **1988**, *196*, 409–430. [CrossRef]
7. Squire, V.A. Ocean wave interactions with sea ice: A reappraisal. *Ann. Rev. Fluid Mech.* **2020**, *52*, 37–60. [CrossRef]
8. Aksenov, Y.; Popova, E.E.; Yool, A.; Nurser, A.J.G.; Williams, T.D.; Bertino, L.; Bergh, J. On the future navigability of Arctic sea routes: High-resolution projections of the Arctic Ocean and sea ice. *Mar. Policy* **2017**, *75*, 300–317. [CrossRef]
9. Tkacheva, L.A. Behavior of a semi-infinite ice cover under a uniformly moving load. *J. Appl. Mech. Tech. Phys.* **2018**, *59*, 258–272. [CrossRef]
10. Sturova, I.V.; Tkacheva, L.A. Wave motion in a fluid under an inhomogeneous ice cover. *J. Phys. Conf. Ser.* **2017**, *894*, 012092. [CrossRef]
11. Plotnikov, P.I.; Toland, J.F. Modelling nonlinear hydroelastic waves. *Philos. Trans. R. Soc. Lond. A Math. Phys. Eng. Sci.* **2011**, *369*, 2942–2956. [CrossRef]
12. Părău, E.I.; Dias, F. Nonlinear effects in the response of a floating ice plate to a moving load. *J. Fluid Mech.* **2002**, *460*, 281–305. [CrossRef]
13. Stepanyants, Y.; Sturova, I. Waves on a compressed floating ice plate caused by motion of a dipole in water. *J. Fluid Mech.* **2021**, *907*, A7. [CrossRef]
14. Stepanyants, Y.; Sturova, I. Hydrodynamic Forces Exerting on an Oscillating Cylinder under Translational Motion in Water Covered by Compressed Ice. *Water* **2021**, *13*, 822. [CrossRef]
15. Il'ichev, A.T. Solitary wave packets beneath a compressed ice cover. *Fluid Dyn.* **2016**, *51*, 327–337. [CrossRef]
16. Amouzadrad, P.; Mohapatra, S.C.; Guedes Soares, C. Hydroelastic Response to the Effect of Current Loads on Floating Flexible Offshore Platform. *J. Mar. Sci. Eng.* **2023**, *11*, 437. [CrossRef]
17. Mohapatra, S.C.; Guedes Soares, C. Effect of mooring lines on the hydroelastic response of a floating flexible plate using the BIEM approach. *J. Mar. Sci. Eng.* **2021**, *9*, 941.
18. Evans, D.V.; Porter, R. Wave scattering by narrow cracks in ice sheets floating on water of finite depth. *J. Fluid Mech.* **2003**, *484*, 143165. [CrossRef]
19. Porter, D.; Evans, D. Diffraction of flexural waves by finite straight cracks in an elastic sheet over water. *J. Fluids Struct.* **2007**, *23*, 309–327. [CrossRef]
20. Tkacheva, L.A. Wave motion in an ice sheet with crack under uniformly moving Load. *Fluid Dyn.* **2019**, *54*, 14–32. [CrossRef]
21. Zeng, L.D.; Korobkin, A.A.; Ni, B.Y.; Xue, Y.Z. Moving load in an ice channel with a crack. *Appl. Ocean. Res.* **2022**, *121*, 103086. [CrossRef]
22. Xue, Y.Z.; Zeng, L.D.; Ni, B.Y.; Korobkin, A.A.; Khabakhpasheva, T.I. Hydroelastic response of an ice sheet with a lead to a moving load. *Phys. Fluids* **2021**, *33*, 037109. [CrossRef]
23. Zhestkaya, V.D. Numerical solution of the problem of an ice sheet under a moving load. *App Mech Tech Phys.* **1999**, *40*, 770–75. [CrossRef]
24. Zhestkaya, V.D.; Kozin, V.M. *Ice Breaking with Air-Cushion Vessels Using a Resonant Method*; Dalnauka: Vladivostok, Russia, 2003; 160p.
25. Brocklehurst, P. *Hydroelastic Waves and Their Interaction with Fixed Structures*; University of East Anglia: Norwich, UK, 2012.
26. Shishmarev, K.A.; Khabakhpasheva, T.I.; Korobkin, A.A. The response of ice cover to a load moving along a frozen channel. *Appl. Ocean Res.* **2016**, *59*, 313–326. [CrossRef]
27. Shishmarev, K.A.; Khabakhpasheva, T.I.; Korobkin, A.A. Ice response to an underwater body moving in a frozen channel. *Appl. Ocean Res.* **2019**, *91*, 101877. [CrossRef]
28. Khabakhpasheva, T.I.; Shishmarev, K.A.; Korobkin, A.A. Large-time response of ice cover to a load moving along a frozen channel. *Appl. Ocean Res.* **2019**, *86*, 154–165. [CrossRef]
29. Ren, K.; Wu, G.X.; Li, Z.F. Hydroelastic waves propagating in an ice-covered channel. *J. Fluid Mech.* **2020**, *886*, A18. [CrossRef]
30. Shishmarev, K.; Zavyalova, K.; Batyaev, E.; Khabakhpasheva, T. Hydroelastic Waves in a Frozen Channel with Non-Uniform Thickness of Ice. *Water* **2022**, *14*, 281. [CrossRef]
31. Li, Q.S.; Cao, H.; Li, G. Static and dynamic analysis of straight bars with variable cross-section. *Int. J. Comput. Struct.* **1996**, *59*, 1185–1191. [CrossRef]

32. Timoshenko, S.; Woinowsky-Krieger, S. *Theory of Plates and Shells*; McGraw-Hill Book Company, Inc.: New York, NY, USA; Toronto, ON, Canada; London, UK, 1959.
33. Pogorelova, A.V.; Zemlyak, V.L.; Kozin, V.M. Moving of a submarine under an ice cover in fluid of finite depth. *J. Hydrodyn.* **2019**, *31*, 562–569. [CrossRef]